PHOTONICS Research

Wavelength-switchable vortex beams based on a polarization-dependent microknot resonator

Jinqiu Zheng,[1] Ao Yang,[1] Teng Wang,[1] Xianglong Zeng,[1,*] Ning Cao,[2] Mei Liu,[2] Fufei Pang,[1] and Tingyun Wang[1]

[1]Key Laboratory of Specialty Fiber Optics and Optical Access Networks, Joint International Research Laboratory of Specialty Fiber Optics and Advanced Communication, Shanghai Institute for Advanced Communication and Data Science, Shanghai University, Shanghai 200444, China
[2]School of Mechatronic Engineering and Automation, Shanghai University, Shanghai 200072, China
*Corresponding author: zenglong@shu.edu.cn

Received 6 December 2017; revised 17 January 2018; accepted 8 February 2018; posted 9 February 2018 (Doc. ID 314915); published 18 April 2018

We experimentally demonstrated a method of generating continuously wavelength-switchable optical vortex beams (OVBs) in an all-fiber laser. A polarization-dependent microknot resonator (MKR) functions as comb filter and accounts for the narrow linewidth (0.018 nm) of multiwavelength channels. The wavelength interval corresponds to the free spectral range of the MKR. We exploit a fused SMF–FMF (single mode fiber–few mode fiber) mode coupler to obtain broadband mode conversion and successfully achieve multiwavelength switchable OVBs. As far as we know, this is the first report about identical multiwavelength vortex beams with topological charges of ±1. It has been verified that each channel of the vortex beams preserves the same orbital angular momentum (OAM) properties through their clear spiral interferograms. Multiwavelength vortex beams with identical OAM properties are desirable for multiplexing, exchanging, and routing to further improve the capacity of optical fiber transmission. © 2018 Chinese Laser Press

OCIS codes: (140.3510) Lasers, fiber; (140.3600) Lasers, tunable; (050.4865) Optical vortices; (060.4230) Multiplexing.

https://doi.org/10.1364/PRJ.6.000396

1. INTRODUCTION

Optical vortex beams (OVBs) are spatially structured beams with a helical phase front. Such beams are characterized by a topological charge (order), also called orbital angular momentum (OAM) beams. Vortex beams have a phase singularity at the center with a doughnut-shaped spatial intensity. Due to their polarization and amplitude symmetry, OVBs attract a lot of attention and have been investigated in many areas, such as high-resolution measurement [1], particle trapping [2], material processing [3], remote sensing [4], microscopy [5], and quantum information technology [6]. OAM recently has been used in applications in multidimensional multiplexing technologies in optical communications, such as wavelength-division multiplexing (WDM), mode-division multiplexing (MDM) [7], and all-optical processes [8]. A traditional method is used to convert a Gaussian beam to a vortex beam using phase elements, such as a *q*-plate [9], or computer-generated holograms created by a programmed spatial light modulator (SLM) [10]. Such phase elements are typically designed for a specific laser wavelength and this inherently constrains the wavelength versatility of the vortex laser sources. Optical vortex modes could be directly generated from a laser cavity by certain methods, such as the use of an annular pump beam for the laser medium [11] and using an SLM as a cavity reflector [12]. Different kinds of vortex lasers based on fiber mode conversion devices have been proposed, such as few-mode fiber Bragg gratings (FBGs) [13–15]. Recently, nonlinear frequency conversion based on optical parametric oscillation [16], optical parametric amplification [17], or stimulated Raman scattering [18,19] is proven to be a valid approach to generate optical vortices in the new waveband. Single-pass optical parametric generation of a Yb-fiber laser was demonstrated to generate optical vortices in the mid-infrared region [20]. However, most of them have two disadvantages: high cost and low integration.

Multiwavelength switchable fiber lasers have the advantages of wavelength flexibility and high coherence. They have been considered excellent sources for optical WDM and sensing systems. Many methods have been proposed to obtain multiwavelength fiber lasers, such as using a Lyot–Sagnac filter [21], a Mach–Zehnder interferometer (MZI) [22], and a superimposed chirped fiber Bragg grating (CFBG) [23]. Zhan *et al.* reported a triple-wavelength switchable lasing laser with equal wavelength spacing of 2.6 nm by using cascaded long-period fiber grating (LPG) [24]. Luo *et al.* reported a wavelength-switchable femtosecond pulse fiber laser using a gold-nanorod saturable absorber (SA) [25].

However, to the best of our knowledge, there have been few reports about a multiwavelength switchable fiber laser with vortex beams. In our prior work, a single-mode fiber (SMF) and few-mode fiber (FMF) coupler was first proposed to overcome the constraint of broadband mode conversion [26,27], which is a promising method to produce efficient femtosecond OVBs. By using a similar fiber mode coupler, cylindrical vector beams with a switchable dual-wavelength pulsed laser were also presented [28]. Multiwavelength vortex beams with identical OAM properties are desirable for multiplexing, exchanging, and routing to further improve the capacity of the optical fiber transmission.

In this paper, we demonstrate a method to experimentally generate multiwavelength switchable and continuously tunable OVBs in an all-fiber laser. A polarization-dependent microknot resonator (MKR), acting for comb filtering and polarization switching, is inserted in the cavity to adjust the wavelength region of net gain. Multiwavelength switchable OVBs with topological charges of $\mathrm{OAM}_{\pm 1}$ can be obtained, and each wavelength channel preserves identical OAM properties.

2. EXPERIMENTAL SETUP

The schematic setup to generate multiple-wavelength OVBs in an all-fiber configuration is shown in Fig. 1. The gain medium of a 40 cm erbium-doped fiber (EDF, LIEKKI ER80-8/125) with group velocity dispersion of −20 $\mathrm{ps}^2/\mathrm{km}$ and peak absorption of 80 dB/m at 1530 nm is pumped by a 980 nm semiconductor laser with the maximum power of 605 mW. A broadband high birefringence Sagnac loop mirror (HiBi-SLM filter) is made of a 50:50 coupler, a section of 15 cm polarization-maintaining fiber (PMF), and two polarization controllers (PCs) (PC1 and PC2) [25]. An optical circulator assures unidirectional operation. The outer ring cavity consists of the MKR (with a red ring structure in the picture), PC3, and an SMF and FMF coupler (coupling ratio 90:10), which is used to convert LP_{01} mode to high-order LP_{11} mode [26,27]. The output spectrum is analyzed by an optical spectrum analyzer (OSA, YOKOGAWA, AQ6370C) and the output beam profiles are recorded using a CCD camera (InGaAs camera, Model C10633-23 from Hamamatsu Photonics).

A. MKR Characteristics

The fiber is tapered by using a flame brushing method to a microfiber of the diameter (approximately 3 μm). Similar to wrapping a rope, the microfiber is manually tied into a knot and then slowly tightened [29]. The diameter of the loop could be further decreased by pulling the fiber ends symmetrically using the stages. The ring diameter of the knot used in the experiment is approximately 660 μm. The microscopy image of the fabricated MKR and the overlapping area are shown in Figs. 2(a) and 2(b). The MKR can be encapsulated for a stable condition. Resonant light is coupled from the fiber and circulating in the MKR.

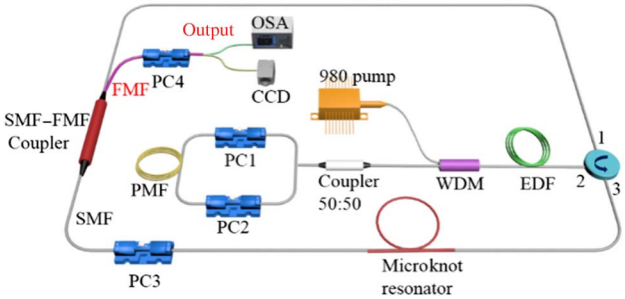

Fig. 1. Experimental setup used to excite OVB pulse. WDM, wavelength division multiplexing coupler; EDF, erbium-doped fiber; PC, polarization controller; OSA, optical spectrum analyzer; CCD, charge-coupled infrared camera; PMF, polarization-maintaining fiber.

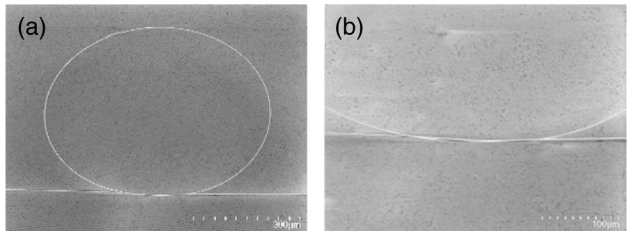

Fig. 2. Microscopy image of (a) the fabricated MKR and (b) the overlapping region.

As shown in Fig. 3(a), the red and the blue lines present the transmission spectra with different incident states of polarization (SOP). The off-resonance loss of the MKR is less than 2.5 dB, and the transmission loss for different SOP is wavelength-dependent. The wavelength resonances of the transmission spectrum keep unchanged and overlapped with different SOP, but their transmission losses are dependent on the incident SOP. The transmissivity difference is large when the wavelengths are near the transmission resonance.

The typical transmission spectra of the MKR with periodic wavelength response covering the whole C-band are shown in Fig. 3(b). The peak-to-notch contrast ratio of the fabricated MKR is around 11 dB, indicating that the MKR is well fabricated, and it also could be further improved by decreasing the surface roughness and changing the diameter of the microfiber. The free spectral range (FSR) is inversely proportional to the perimeter of MKR. Here, the measured FSR is 0.813 nm, which is consistent with the calculated result, $\mathrm{FSR} = \lambda^2/n\pi D$ [30]. The polarization dependent loss (PDL) of the MKR has been measured using a tunable laser and a polarization analyzer. Due to the lack of circular symmetry, the coupling in the overlapping regions of the MKR is highly polarization-dependent. Figure 3(c) shows the PDL of the MKR from 1530 nm to 1570 nm, which is the maximum transmission difference (up to 7 dB) near the resonant wavelengths under all polarization states. The transmission spectra exhibit unequal variations with different incident SOP.

B. Generating OAM Based on Fused SMF–FMF Couplers

To obtain OVBs, a fused SMF–FMF fiber coupler, which acts as a mode converter, has been investigated [26]. When propagation constant β_1 of LP_{01} mode in SMF equals the propagation constant β_2 of LP_{11} mode in FMF, LP_{01} mode in SMF can be phase-matched and converted to LP_{11} mode in FMF according to the coupled-mode theory [31]. LP_{11} mode is actually the superposition of vector modes, $\mathrm{TE}_{0,1}$, $\mathrm{TM}_{0,1}$ and $\mathrm{HE}_{2,1}^{\mathrm{even}}$ ($\mathrm{HE}_{2,1}^{\mathrm{odd}}$). And OAM optical vortex can be obtained by

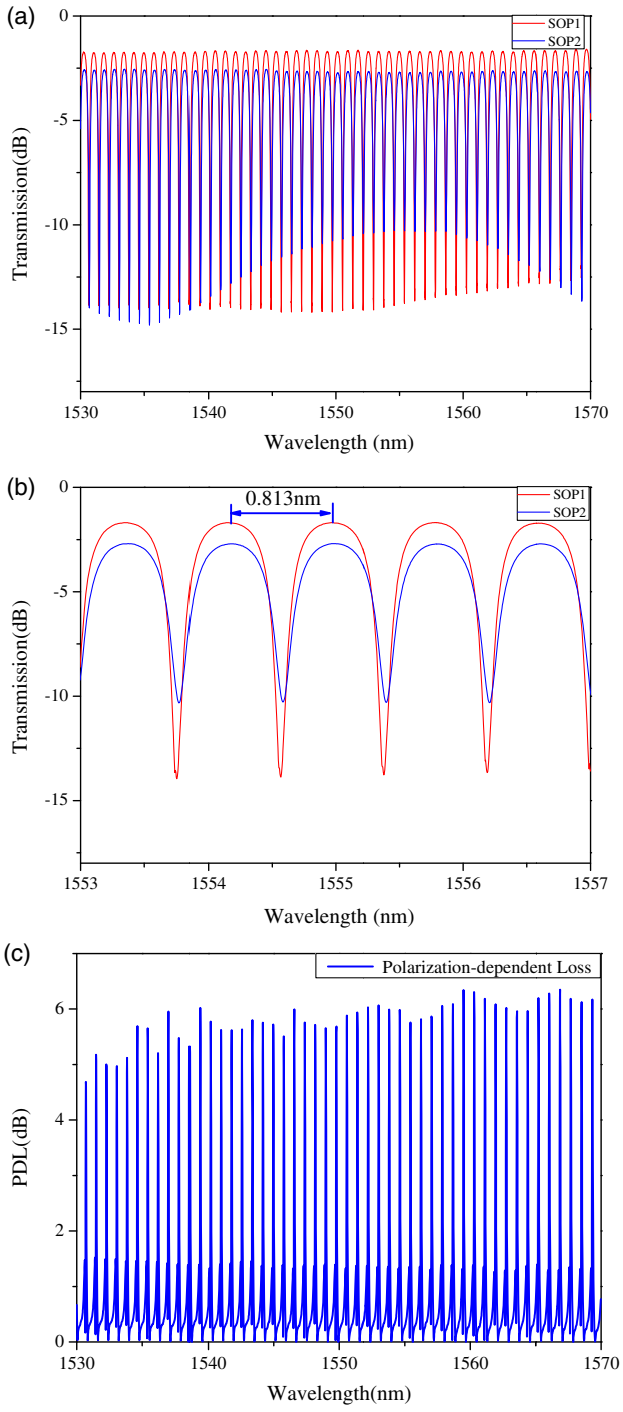

Fig. 3. Spectral response of MKR: (a) Transmission spectrum with different incident states of polarization (SOP); (b) transmission spectra from 1553 nm to 1557 nm; and (c) polarization-dependent loss of the MKR.

combining different vector modes $HE_{2,1}^{even}(HE_{2,1}^{odd})$ and $TE_{0,1}$ ($TM_{0,1}$) when $l = 1$, or combining $HE_{l+1,m}^{even}$ ($HE_{l+1,m}^{odd}$) and $EH_{l-1,m}^{even}$ ($EH_{l-1,m}^{odd}$) when $l > 1$ with a $\pi/2$ phase shift, where l refers to the azimuthal index and m refers to the radial index [32]. Then a $\pi/2$ phase shift between two vector modes is an indispensable part of generating OAM OVBs. A polarization controller (PC4) is used to achieve a $\pi/2$ phase shift between vector modes.

The commercial simulation software (Rsoft) is used to solve the modes propagating in the SMF–FMF couplers. The simulation results are shown in Fig. 4. SMF and FMF core diameters are set to 5.60 μm and 10.90 μm, respectively. The corresponding mode effective indices are 1.444. The coupling region length is set to 2300 μm, and the core distance between the two fibers is set to 5 μm. The conversion efficiency is the ratio of LP_{01} mode in SMF coupled to LP_{11} mode in FMF as a function of the wavelengths, as shown in Fig. 4(a). The coupling efficiency is more than 95% from 1507 nm to 1595 nm. Figure 4(b) shows the power exchange in the coupling region when LP_{01} mode from the SMF converts to LP_{11} mode in the FMF at the wavelength of 1520, 1550, and 1580 nm, respectively.

Before the fusing process of the SMF–FMF fiber coupler, SMF (core/cladding diameter = 8/125 μm) is pre-tapered to the cladding diameter of around 85 μm, while the core/cladding diameter of FMF fiber is 20/125 μm. Then the pre-tapered SMF and FMF are twisted, stretched, and fused together using an oxyhydrogen flame so that their fiber core diameters are near to the phase-matching condition. Optimum taper diameters are determined after experimental fine tuning of pre-tapered SMF diameters [26]. The powers from the output SMF port and FMF port are carefully monitored. The coupling ratio (CR) is expressed by the ratio between the out power in FMF (P_2) and the total output power of SMF (P_1) and FMF (P_2): $CR = P_2/(P_1 + P_2)$. When the desired coupling ratio is achieved, the automated fusing and pulling process is stopped. The change of the power coupling is observed during the fiber pulling and fusing process, and a different splitting ratio can be obtained by controlling the pulling length.

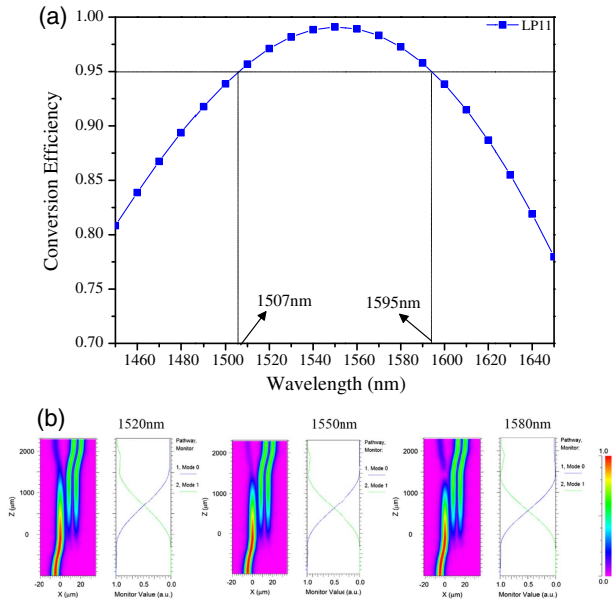

Fig. 4. Simulation results: (a) Coupling efficiency as a function of the wavelengths; and (b) power exchange in the coupling region when LP_{01} mode in SMF converts to LP_{11} mode in FMF.

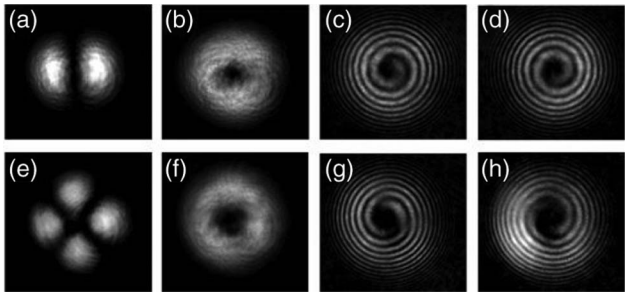

Fig. 5. Output near-field intensity distribution from a mode selective coupler by inputting a femtosecond pulse. (a), (e) Intensity profiles of the LP_{11} and LP_{21} modes; (b), (f) donut-shaped OAM mode patterns when pressing the output FMF; (c) and (d), and (g) and (h) corresponding clockwise and anticlockwise spiral interferograms of $OAM_{\pm1}$ and $OAM_{\pm2}$, respectively.

Fiber $OAM_{\pm1}$ modes can be obtained by combining vector modes $HE_{2,1}^{even}$ ($HE_{2,1}^{odd}$) and $TE_{0,1}$ ($TM_{0,1}$) with a $\pi/2$ phase shift [32]. By rotating the PC4 on the output of FMF and adjusting the pressure appropriately, a $\pi/2$ phase shift between vector modes can be achieved. The mode selective coupler with a broad bandwidth is further verified by inputting a femtosecond pulse with a spectrum bandwidth of 32 nm (centered at 1550 nm) and its pulse duration is around 150 fs. Femtosecond optical vortex beams are obtained from the FMF output port of the mode selective coupler, as shown in Fig. 5. The output high-order mode patterns and the corresponding interference patterns of $OAM_{\pm1}$, $OAM_{\pm2}$ modes are clearly seen, respectively, which indicate that the mode selective coupler can work as an efficient mode converter within a large bandwidth.

3. RESULTS AND DISCUSSION

The mechanism of wavelength-switchable fiber laser is easy to explain. The MKR comb filter exhibits a polarization-dependent transmission loss for different wavelengths, which leads to unequal cavity losses at the lasing wavelength channels. Due to the existence of mode competition in erbium-doped fiber, a small change of cavity loss can lead to the different lasing wavelengths. By adjusting the state of polarization of the PCs to change the transmission loss of the MKR cavity, it leads to unequal cavity losses at the lasing wavelength channels. The wavelength-switching operation can be obtained for different wavelengths. To extend the tuning range, a broadband HiBi-SLM filter is used. It is known that its reflective spectrum is a periodic sinusoidal curve, and the reflective bandwidth is inversely proportional to the PMF length. In fact, only the gain at the wavelengths near the center of the reflective profile of the HiBi–SLM filter can offset the cavity loss to generate the lasing. The PMF length is about 15 cm and its reflective bandwidth is about 30 nm. Moreover, the effective gain region can be tuned along with the reflective profile [33], which is first tuned by adjusting the PC1 and PC2 to the desired lasing band. Then the SOP of the MKR is adjusted to switch the lasing wavelengths continuously by using PC3.

Multiwavelength switchable lasing based on the MKR is demonstrated experimentally, as shown in Fig. 6. By adjusting the PCs appropriately, adjacent single- and dual-wavelength outputs are successively tuned out in the lasing channels. The signal-to-noise ratio (SNR) of each channel keeps as higher

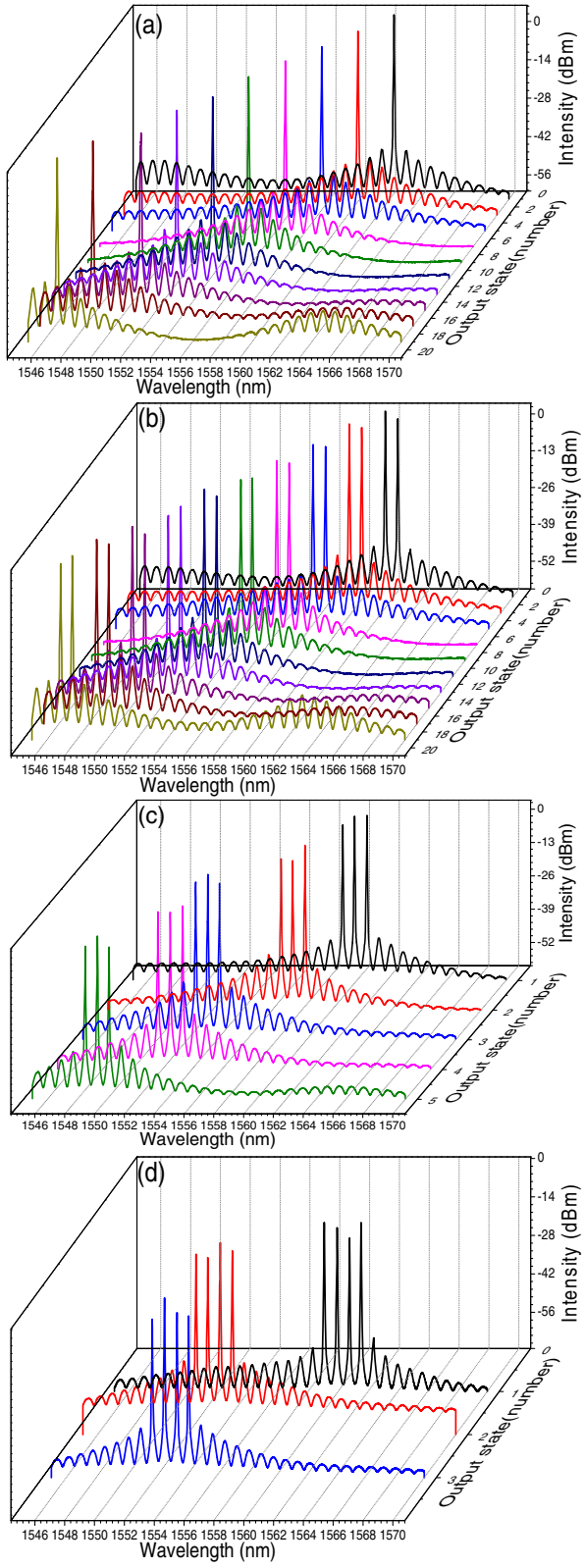

Fig. 6. Output spectra of successively tunable (a) single-, (b) dual-, (c) triple-, and (d) quadruple-wavelength lasing operations.

than 40 dB, which is mainly attributed to the high contrast of the comb spectrum of the MKR (Fig. 3). Moreover, the measured 3 dB linewidth of each channel reaches approximately 0.018 nm, limited by the measurement of OSA precision. Single-longitudinal-mode oscillation can be realized based on a fiber Fabry–Perot interferometer and the MKR in the state of single-wavelength lasing [34]. The wavelength interval is 0.813 nm, which is in agreement with the FSR of the MKR. As shown in Fig. 6(a), the single wavelength can be tuned from 1546.95 nm to 1562.29 nm, and continuous 19 wavelengths in total are generated. Then multiwavelength operation is achieved based on these wavelengths. The output spectra of more multiwavelength lasing are observed. As shown in Figs. 6(b)–6(d), stable adjacent dual-, triple- and quadruple-wavelength channels can also be tuned continuously through controlling the polarization state of light inside the HiBi-SLM filter, the MKR, and the fiber ring cavity.

The proposed multiwavelength switchable fiber laser exhibits some advantages. First, multiwavelength channels can be flexibly tuned with different number combinations of lasing channels, which cover versatile single-, dual-, triple-, and quadruple-wavelength lasing. Second, it is a compact and simple configuration of a polarization-dependent MKR and a HiBi-SLM filter, which offers comb filtering and polarization switching.

We also investigate the generation stability of multiwavelength lasing channels. The output triple-wavelength spectra are repeatedly scanned every minute, as shown in Fig. 7(a). The output power can be increased by reducing the whole cavity loss or increasing the power of pump or even double pump configuration. Here, the output power of the vortex beams is about 2 mW. The fluctuation of output power is less than 2.5 dBm, and central wavelengths of different channels remain within 0.03 nm in 10 min, which show the stability of the output laser, as shown in Fig. 7(b).

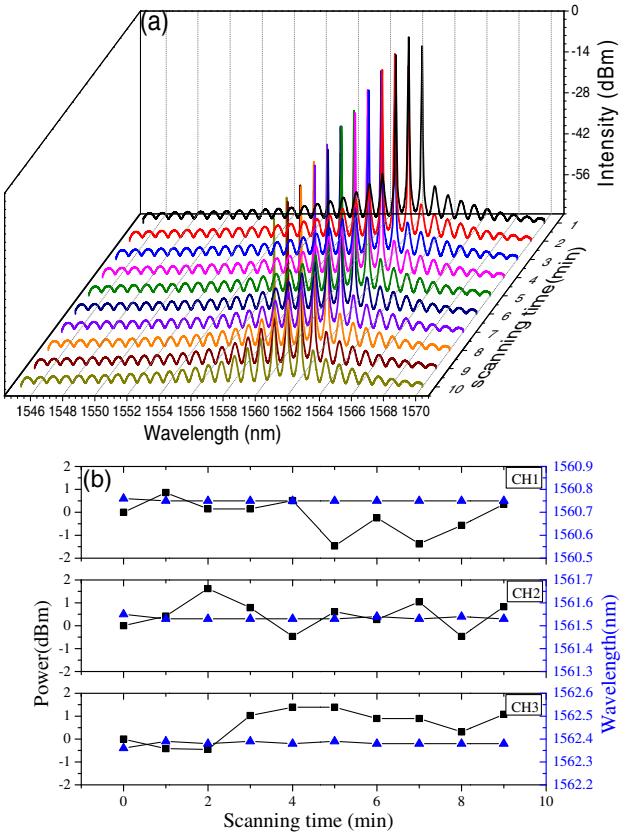

Fig. 7. Stability of triple-wavelength output spectrum. (a) Repeat scans of triple-wavelength output spectrum every minute. (b) Power fluctuation (black) and central wavelength (blue) of each channel in the triple-wavelength output every minute.

We further exploit the polarization characteristics of multiwavelength switchable outputs through a fused SMF–FMF coupler inserted in the cavity. The mode patterns from the FMF output of the broadband mode coupler are observed when the fiber laser is running at the state of switchable wavelengths. The fused SMF–FMF coupler has been verified effectively when acting as a mode selective converter. A polarizer is added before the CCD camera; by rotating the polarization direction, linearly polarized vortex beams are observed.

We show in Fig. 8 that four columns present the experimental near-field intensity patterns of the LP_{11} mode and the corresponding $OAM_{\pm 1}$ of a single wavelength (1559.09 nm), dual wavelengths (1559.09 nm and 1559.90 nm), triple wavelengths (1559.09, 1559.90, and 1560.71 nm), and quadruple wavelengths (1559.09, 1559.90, 1560.71, and 1561.52 nm), respectively. Figures 8(a) and 8(b) are the experimental near-field patterns of LP_{11} mode and the donut-shaped mode pattern when adjusting the PC4 on the FMF output. Figures 8(c) and 8(d) are the corresponding clockwise and anticlockwise spiral interferograms. Figure 8(e) is the output spectrum of the single-wavelength lasing operation. Other columns present

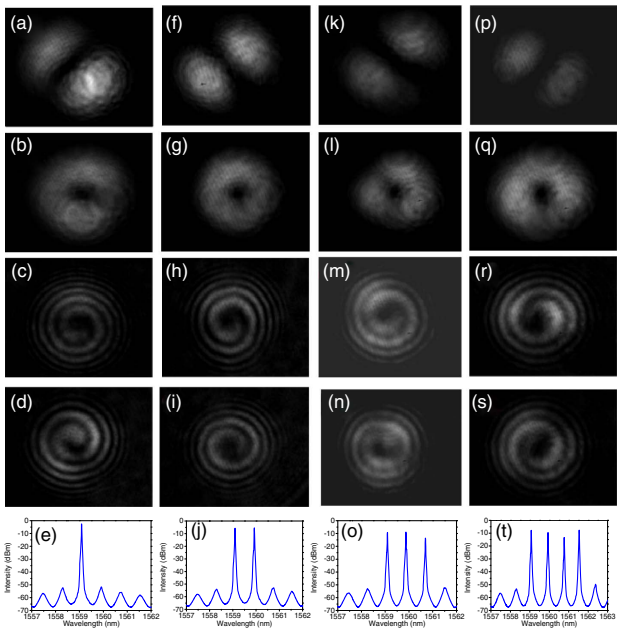

Fig. 8. Near-field distribution of LP_{11} intensities, OAM patterns, spiral interferograms, and the out spectra of wavelength-switchable laser. Four columns present (a)–(e) single-, (f)–(j) dual-, (k)–(o) triple-, and (p)–(t) quadruple-wavelength lasing operations. First row, LP_{11} intensity profiles; second row, donut-shaped mode patterns of vortex beams; third and fourth rows, corresponding clockwise and anticlockwise spiral interferograms; and fifth row, the output spectra.

the experimental results of dual-, triple- and quadruple-wavelength lasing operations. The purities of the modes are estimated to be more than 95% using the tight bend approach [35].

The clockwise and counterclockwise spiral interference patterns indicate the vortex beams with OAM_{-1} and OAM_{+1}. LP_{11} and OAM mode intensities are preserved identically between the multiwavelength channels and keep the same polarization properties, which are due to the polarization switching of the MKR and HiBi–SLM filter. The near-field LP_{11} mode intensity patterns, the vortex patterns, and their corresponding spiral interferograms of adjacent single, dual, triple, and quad wavelengths are clearly observed without any distortion. It is concluded that each wavelength channel carries identical properties of OAM_{+1} or OAM_{-1}.

We successfully obtain multiwavelength vortex beams with identical OAM properties, which are desirable for multiplexing, exchanging, and routing to further improve the capacity of optical fiber transmission. The multiwavelength switchable lasing shows a potential application in mode-division multiplexing, OAM modes switching, and routing.

4. CONCLUSION

In conclusion, we experimentally demonstrate a method to generate multiple-wavelength switchable OVBs in an all-fiber laser based on a polarization-dependent MKR. The tuning wavelengths range from 1546 nm to 1562 nm, and single-, dual-, triple-, and quadruple-wavelength channels can be switched. The wavelength interval is 0.813 nm, which is in agreement with the FSR of the MKR. Variable wavelength intervals can be acquired by just changing the diameter of the MKR. We use a fused SMF–FMF mode coupler to successfully obtain broadband mode conversion and achieve multiwavelength switchable OVBs. It also verifies that each wavelength channel preserves identical OAM properties through their clear spiral interferograms. The proposed wavelength-switchable and widely tunable OAM fiber laser may be useful in various fields, such as mode-division multiplexing, optical fiber communication, and material processing.

Funding. National Natural Science Foundation of China (NSFC) (91750108, 61635006); Science and Technology Commission of Shanghai Municipality (STCSM) (16520720900); Shanghai Education Development Foundation (SHEDF) (16SG35).

Acknowledgment. X. Zeng acknowledges the support of the Program for Professor of Special Appointment (Eastern Scholar) at Shanghai Institutions of Higher Learning and Science and Technology Commission of Shanghai Municipality. F. Pang was supported by the Shuguang Program of Shanghai Education Development Foundation and Shanghai Municipal Education Commission.

REFERENCES

1. L. Novotny, M. R. Beversluis, K. S. Youngworth, and T. G. Brown, "Longitudinal field modes probed by single molecules," Phys. Rev. Lett. **86**, 5251–5254 (2001).
2. H. Kawauchi, K. Yonezawa, Y. Kozawa, and S. Sato, "Calculation of optical trapping forces on a dielectric sphere in the ray optics regime produced by a radially polarized laser beam," Opt. Lett. **32**, 1839–1841 (2007).
3. M. Meier, V. Romano, and T. Feurer, "Material processing with pulsed radially and azimuthally polarized laser radiation," Appl. Phys. A **86**, 329–334 (2007).
4. G. Milione, T. Wang, J. Han, and L. Bai, "Remotely sensing an object's rotational orientation using the orbital angular momentum of light," Chin. Opt. Lett. **15**, 030012 (2017).
5. S. W. Hell and J. Wichmann, "Breaking the diffraction resolution limit by stimulated emission: stimulated-emission-depletion fluorescence microscopy," Opt. Lett. **19**, 780–782 (1994).
6. A. Nicolas, L. Veissier, L. Giner, E. Giacobino, D. Maxein, and J. Laurat, "A quantum memory for orbital angular momentum photonic qubits," Nat. Photonics **8**, 234–238 (2014).
7. N. Bozinovic, Y. Yue, Y. Ren, M. Tur, P. Kristensen, H. Huang, A. E. Willner, and S. Ramachandran, "Terabit scale orbital angular momentum mode division multiplexing in fibers," Science **340**, 1545–1548 (2013).
8. S. Zhu, L. Shi, S. Yuan, X. Xu, and X. Zhang, "All-optical control of ultrahigh-Q silica microcavities with iron oxide nanoparticles," Opt. Lett. **42**, 5133–5136 (2017).
9. F. Cardano, E. Karimi, S. Slussarenko, L. Marrucci, C. de Lisio, and E. Santamato, "Polarization pattern of vector vortex beams generated by q-plates with different topological charges," Appl. Opt. **51**, C1–C6 (2012).
10. S. Ramachandran, P. Kristensen, and M. F. Yan, "Generation and propagation of radially polarized beams in optical fibers," Opt. Lett. **34**, 2525–2527 (2009).
11. J.-F. Bisson, Y. Senatsky, and K.-I. Ueda, "Generation of Laguerre–Gaussian modes in Nd:YAG laser using diffractive optical pumping," Laser Phys. Lett. **2**, 327–333 (2005).
12. A. Forbes, "Controlling light's helicity at the source: orbital angular momentum states from lasers," Philos. Trans. R. Soc. London Ser. A **375**, 20150436 (2017).
13. J. Dong and K. S. Chiang, "Mode-locked fiber laser with transverse-mode selection based on a two-mode FBG," IEEE Photon. Technol. Lett. **26**, 1766–1769 (2014).
14. B. Sun, A. Wang, C. Gu, G. Chen, L. Xu, D. Chung, and Q. Zhan, "Mode-locked all-fiber laser producing radially polarized rectangular pulses," Opt. Lett. **40**, 1691–1694 (2015).
15. D. Mao, T. Feng, W. Zhang, H. Lu, Y. Jiang, P. Li, B. Jiang, Z. Sun, and J. Zhao, "Ultrafast all-fiber based cylindrical-vector beam laser," Appl. Phys. Lett. **110**, 021107 (2017).
16. T. Yusufu, Y. Tokizane, M. Yamada, K. Miyamoto, and T. Omatsu, "Tunable 2-μm optical vortex parametric oscillator," Opt. Express **20**, 23666–23675 (2012).
17. K. Miyamoto, K. Suizu, T. Akiba, and T. Omatsu, "Direct observation of the topological charge of a terahertz vortex beam generated by a Tsurupica spiral phase plate," Appl. Phys. Lett. **104**, 261104 (2014).
18. A. J. Lee, T. Omatsu, and H. M. Pask, "Direct generation of a first-stokes vortex laser beam from a self-Raman laser," Opt. Express **21**, 12401–12409 (2013).
19. A. J. Lee, C. Zhang, T. Omatsu, and H. M. Pask, "An intracavity, frequency-doubled self-Raman vortex laser," Opt. Express **22**, 5400–5409 (2014).
20. A. Aadhi, V. Sharma, R. P. Singh, and G. K. Samanta, "High-power, high repetition rate, tunable, ultrafast vortex beam in the near-infrared," J. Opt. **20**, 01LT01 (2018).
21. Y. G. Han, G. Kim, J. H. Lee, S. H. Kim, and S. B. Lee, "Lasing wavelength and spacing switchable multiwavelength fiber laser from 1510 to 1620 nm," IEEE Photon. Technol. Lett. **17**, 989–991 (2005).
22. A. P. Luo, Z. C. Luo, and W. C. Xu, "Tunable and switchable multiwavelength erbium-doped fiber ring laser based on a modified dual-pass Mach–Zehnder interferometer," Opt. Lett. **34**, 2135–2137 (2009).
23. X. Y. Dong, P. Shum, N. Q. Ngo, and C. C. Chan, "Multiwavelength Raman fiber laser with a continuously-tunable spacing," Opt. Express. **14**, 3288–3293 (2006).

24. M. Yan, S. Y. Luo, L. Zhan, Z. M. Zhang, and Y. X. Xia, "Triple-wavelength switchable erbium-doped fiber laser with cascaded asymmetric exposure long-period fiber gratings," Opt. Express **15**, 3685–3691 (2007).
25. X. Wang, Z. Luo, M. Liu, R. Tang, A. Luo, and W. Xu, "Wavelength-switchable femtosecond pulse fiber laser mode-locked by silica-encased gold nanorods," Laser Phys. Lett. **13**, 045101 (2016).
26. T. Wang, F. Wang, F. Shi, F. Pang, S. Huang, T. Wang, and X. Zeng, "Generation of femtosecond optical vortex beams in all-fiber mode-locked fiber laser using mode selective coupler," J. Lightwave Technol. **35**, 2161–2166 (2017).
27. F. Wang, F. Shi, T. Wang, F. Pang, T. Wang, and X. Zeng, "Method of generating femtosecond cylindrical vector beams using broadband mode converter," IEEE Photon. Technol. Lett. **29**, 747–750 (2017).
28. Z. Zhang, Y. Cai, J. Wang, H. Wan, and L. Zhang, "Switchable dual-wavelength cylindrical vector beam generation from a passively mode-locked fiber laser based on carbon nanotubes," IEEE J. Sel. Top. Quantum Electron. **24**, 1100906 (2018).
29. L. Xiao and T. A. Birks, "High finesse microfiber knot resonators made from double-ended tapered fibers," Opt. Lett. **36**, 1098–1100 (2011).
30. K. S. Lim, S. W. Harun, S. S. A. Damanhuri, A. A. Jasim, C. K. Tio, and H. Ahmad, "Current sensor based on microfiber knot resonator," Sens. Actuators A Phys. **167**, 60–62 (2011).
31. Y. L. Xiao, Y. G. Liu, W. Zhi, Z. Wang, and X. Q. Liu, "Design and experimental study of mode selective all fiber fused mode coupler based on few mode fiber," Acta Phys. Sin. **64**, 204207 (2015).
32. Y. Jiang, G. Ren, Y. Lian, B. Zhu, W. Jin, and S. Jian, "Tunable orbital angular momentum generation in optical fibers," Opt. Lett. **41**, 3535–3538 (2016).
33. X. Liu, L. Zhan, S. Luo, Y. Wang, and Q. Shen, "Individually switchable and widely tunable multiwavelength erbium-doped fiber laser based on cascaded mismatching long-period fiber gratings," J. Lightwave Technol. **29**, 3319–3326 (2011).
34. Z. Xu, Y. Luo, Q. Sun, Y. Xiang, P. P. Shum, and D. Liu, "Switchable single longitudinal-mode fiber laser based on θ-shaped microfiber filter," IEEE Photon. Technol. Lett. **30**, 479–482 (2017).
35. R. Ismaeel, T. Lee, B. Oduro, Y. Jung, and G. Brambilla, "All-fiber fused directional coupler for highly efficient spatial mode conversion," Opt. Express **22**, 11610–11619 (2014).